In situ redeposition of trace metals mobilized by CO2-charged brines

M. Wigley, N. Kampman, H.J. Chapman, Benoît Dubacq, M.J. Bickle

In-situ re-deposition of trace metals mobilized by CO_2-charged fluids

M. Wigley[1], N. Kampman[1], H. C. Chapman[1], B. Dubacq[1], and M. J. Bickle[1]

Corresponding author: M Wigley, Department of Earth Sciences, University of Cambridge, Downing Street, Cambridge, CB2 3EQ, UK (mmw36@cam.ac.uk).

[1]Department of Earth Sciences,

University of Cambridge, Cambridge, UK.

Abstract. Mobilization of contaminants by CO_2-charged brines is one concern relating to injection of CO_2 as part of carbon capture and storage projects. This study monitors the mobility of trace metals in an exhumed CO_2-charged aquifer near the town of Green River, Utah (USA), where CO_2-charged brines have bleached red sandstones, and concentrated trace metals at the bleaching reaction front. Mass balance calculations on the trace metal enrichments are used to calculate time-integrated fluid fluxes and show that a significant fraction of the metals mobilized by the CO_2-rich fluids are re-deposited locally. A sequential extraction procedure on metal-enriched samples shows that these metals are incorporated into secondary carbonate and oxide phases which have been shown to grow at the CO_2-promoted bleaching reaction front. We argue that whilst CO_2-charged fluids are capable of mobilizing trace metals, local metal re-deposition implies that the potential for contamination of overlying freshwater aquifers is low.

1. Introduction

Geological CO_2 sequestration is proposed as one method for mitigating the effects of fossil fuel burning on global climate [e.g. *IPCC*, 2007]. One of the outstanding scientific questions relates to the potential for injected CO_2 to leak and contaminate overlying freshwater aquifers [*Gale*, 2004; *Smyth et al.*, 2009]. CO_2, injected into geological formations in a gaseous or supercritical state, is likely to dissolve into formation fluids at the gas-water contact forming acid brines [*Bickle*, 2009]. These brines can mobilize trace metals via desorption of metals bound to mineral surfaces, or by dissolution of trace metal-bearing phases [*Yin et al.*, 1996; *Bradl*, 2004]. If these brines were to migrate into overlying freshwater aquifers, there is concern that drinking water supplies could be affected. Models [*Wilkin and DiGiulio*, 2010; *Zheng et al.*, 2009] and experiments [*Little and Jackson*, 2010; *Lu et al.*, 2010] have shown that CO_2 can mobilize trace metals; however field experiments have not shown hazardous levels of contamination [*Keating et al.*, 2010; *Kharaka et al.*, 2010]. Of critical importance for environmental contamination is whether the majority of mobilized metals remain in solution or are re-deposited locally.

CO_2 has been escaping along the Little Wash and Salt Wash grabens for hundreds of thousands of years [*Kampman et al.*, 2009, 2012; *Dockrill and Shipton*, 2010]. Near the town of Green River, Utah, red sandstones have been bleached by CO_2-charged brines which have dissolved hematite grain coatings, with trace metals released from the grain coatings concentrated at the bleaching reaction front [*Wigley et al.*, 2012]. The CO_2-promoted reaction fronts are used as an analogue for processes occurring in modern CO_2 injection sites if injected CO_2 were to leak into overlying aquifers. Here we quantify trace

metal enrichments at the bleaching reaction fronts, and use these to calculate corresponding time-integrated fluid fluxes (TIFF; *Bickle and Baker*, 1990) and the fraction of trace metals which have been re-deposited at the reaction front.

1.1. Green River natural analogue site

Within the field area, the Jurassic Entrada sandstone is a well sorted sediment of uniform grain size and mineralogy. Regional burial diagenesis includes the development of Fe-oxide grain coatings [*Cullers*, 1995; *Trimble*, 1978], giving the rock its red color. Near the town of Green River, Utah, the Entrada sandstone has been bleached a pale yellow by diagenetic fluids which have dissolved the Fe-oxide grain coatings [*Wigley et al.*, 2012]. Bleaching occurs at the base of the formation in a broad domal structure, exposed over a 1-2km east-west section along the Salt Wash graben, at the crest of the Green River anticline (Fig. 1a).

Several lines of evidence suggest that the bleaching fluid was a CO_2-charged brine with minor methane, distinguishing the Green River bleaching from hydrocarbon-related bleached sandstones elsewhere on the Colorado Plateau [*Wigley et al.*, 2012; *Beitler et al.*, 2003, 2005]. Carbonates associated with the Green River bleaching have a heavier carbon isotopic composition than documented occurrences of hydrocarbon related bleaching [*Wigley et al.*, 2012]. These values are similar to those measured in the actively leaking CO_2-system near Green River [*Assayag et al.*, 2009], but are inconsistent with isotopically light methane bearing fluids. Mobilization of low pH-soluble trace metals is also inconsistent with methane-rich fluids which have pH $\approx$7.5 when saturated with hematite (Supplementary figure 1). The occurrence of the bleaching at the base of the stratigraphy also rules out buoyant methane bearing fluids as the cause of the alteration. Raman

spectroscopy of fluid inclusions hosted in aragonite, quartz overgrowths and gypsum, petrographically linked to the bleaching suggests that the bleaching fluid was a low temperature (≈27°C) brine (salinity 2-5-7 wt%) with the vapor phase consisting dominantly of CO_2, with minor (0-28%) methane present in three inclusions [*Wigley et al.*, 2012]. The magnitude of the Fermi-diad separation in the Raman spectra of CO_2 is calibrated for the pressure of CO_2 in the vapor phase at high temperatures [*Rosso and Bodnar*, 1995]. An extrapolation to calculated temperatures during bleaching suggests that the bleaching fluid had a CO_2 partial pressure of 1.8-25.9±9.7 bar (Figure 2).

The upper bleached-red contact is well exposed and is sharp and sub-horizontal [*Wigley et al.*, 2012] except in regions of fractures and granulation seams, where differences in porosity and tortuosity enhance or retard vertical transport of the reaction front, respectively (Fig. 1b-c; *Wigley et al.*, In Press). The lower contact appears less sharp but is rarely exposed. To the East the bleached zone terminates as a series of meter scale fingers into red sandstones, whilst the western extent is not exposed. It is thought that the CO_2-rich fluid migrated as a gravity current, with the main components of flow to the north along the plunge of the anticline, and to the east, down dip and in the direction of regional groundwater flow [*Kampman et al.*, 2009], with vertical transport dominated by diffusion except in areas containing faults and open fractures (Fig. 1b; *Wigley et al.* 2012).

Analyses of profiles across the upper sub-horizontal contact between red and bleached sandstone show enrichments in bulk rock trace metal content within 10 cm of the contact (Fig. 3a-f; raw data and sample localities are given in supplementary tables 1 and 2), thought to originate from release of trace metals as grain coating Fe-oxides were dissolved,

with subsequent re-deposition at the reaction front [*Wigley et al.*, 2012]. These trace metals are soluble at low pH, becoming insoluble as pH rises across the reaction front. The scale of enrichments is determined by the volume of fluid that interacted with the reaction front, which had previously reacted with unaltered rock.

Bleaching also occurs around open fractures (Fig 1c), which are mineralized with carbonate and Fe-oxides, and exhibits the same geochemical, isotopic and petrological signatures as the sub-horizontal bleaching contacts [*Wigley et al.*, 2012], indicating a common parent fluid reservoir and continuity in reactive-transport processes. The fracture-associated bleaching reaction front began within the plane of the fracture and migrated laterally by diffusion and advection of the fluid. The asymmetry of the bleached halos is due to the diffusion away from the fractures being imposed on uni-directional horizontal regional flow in the aquifer. Spikes in heavy metal concentration are observed near to the red-bleached transition (Fig. 3a-f), similar to those across horizontal contacts. These observed enrichments of trace metals away from bleached fractures may be related to deposition of metals released by the bleaching reaction front as it moves outwards from the fracture, and/or metals present in the bleaching fluid as it enters the fracture.

Key questions include: (1) what was the original distribution of the metals? (2) How, and in which phases, are the metals re-deposited? (3) What fraction of the mobilized metals is subsequently re-deposited? (4) Does the concentration of metals in the fluid reach levels hazardous for human health?

2. Methods

2.1. Sampling and analytical methods

Profiles from bleached to unbleached sandstones were cored using an electric diamond-edged 40mm core plug drill, with samples spaced at 2-15cm intervals. Core plugs near to the bleached-red contact were sub-sampled every 4mm using a 2mm tungsten-carbide drill bit. Between drilling, the bit and core were cleaned with compressed air. Samples were dissolved in HF and HNO_3 using an open beaker method, and analyzed by inductively coupled plasma-atomic emission spectroscopy (major elements), and ICP-mass spectrometry (trace elements) in Cambridge, UK.

2.2. Mass of metals in enriched zones

The mass of a metal in the enriched region is calculated by integrating across the enriched zone, assuming a stepped concentration profile. Uncertainties are estimated by propagating the uncertainties on the background and enriched compositions. The background compositions are taken as the average within the bleached zone (bleached sandstone), and the average composition of red sandstone near to the bleached fracture (unaltered sandstone; 1σ uncertainty, background compositions are given in supplementary table 4). The uncertainty in peak height is propagated 1σ instrument uncertainty, 1σ of repeat analyses and recovery relative to USGS standard Sco-1 (Supplementary table 1). The range in the fraction of each metal re-adsorbed is calculated from a Monte-Carlo simulation (n=1000) where each parameter listed above is allowed to vary within its range in uncertainty. The range in the fraction of each metal re-deposited is given by 1σ about the mean of the resulting distribution.

2.3. Sequential extraction

The nature of the minerals hosting the re-deposited metals was determined by a sequential extraction procedure (modified from *Tessier et al.* [1979] and *Förstner* [1982]) applied to a selection of unaltered and bleached samples and to metal-enriched samples from sub-horizontal reaction fronts. Leaching was performed at room temperature in 5 steps: (1) Water rinse: 1.5mL de-ionized 18MΩ water with continuous agitation for 2 hours. (2) Exchangeable fraction: 1.5mL 1M sodium acetate solution (NaOAc) at pH 8.2, with continuous agitation for 3 hours. (3) Carbonates: 1.5mL 1M NaOAc adjusted to pH 5 with acetic acid (HOAc), with continuous agitation for 7 hours, repeated 3 times. (4) Oxides: 1.5mL 0.1M oxalate buffer adjusted to pH 3 with oxalic acid. Occasional agitation for 54 hours, repeated 3 times. (5) HCl rinse (remaining carbonate/oxides): 1.5mL 16M HCl with continuous agitation for 2.5 hours.

After each leach the sample was centrifuged for 30 minutes at 3000 rpm, and the liquid pipetted carefully into a cleaned centrifuge tube. The sample was then rinsed with MΩ water, re-centrifuged, and the rinse added to the leachate solution. After the final leaching step, the residue was dried down and dissolved in a combination of HF and HNO_3 in an open beaker method. The leachate solutions were evaporated to dryness and re-dissolved in a dilute nitric acid solution.

The number of moles of a mineral phase dissolved in each sequential leaching step was determined by a modal decomposition of the compositions of the leachate solutions. This was done by minimizing the difference between theoretical and observed compositions by varying the moles of each mineral dissolved. Mineral compositions of plagioclase, K-feldspar and carbonates are taken from electron microprobe analyses (supplementary

table 5). An average clay composition is used based on the major element chemistry of the <2μm fraction ($Al_{1.4}Ca_{0.2}Fe_{0.5}K_{0.8}Mg_{0.2}Na_{0.2}Si_{3.8}O_{10}(OH)_2$; recalculated to an 12 oyygen formula). Fe and Ti-oxides, pyrite and quartz are assumed to exist as pure phases.

3. Results and discussion

3.1. Phases dissolved during sequential extraction

The results of the modal decomposition of sequential leaching solutions are shown in table 1. The water rinse predominantly dissolves soluble salts, releasing up to 86% of available S with a Ca/S ratio of $\approx$ 1. Modal analysis on water rinse solutions shows that 75% of all minerals dissolved in this step are gypsum (table 1). The exchangeable leach removes residual soluble salts and minor amounts of calcite and silicates. It also removes loosely adsorbed cations: in some samples up to 60% of total Sr is removed in this step. Up to 80% total Ca and 60% total Mg are removed in the carbonate leach indicating dissolution of calcite and dolomite. Approximately 95% of minerals dissolved are carbonates. The oxide leach removes up to 60% of total Fe with a greater fraction released in bleached samples, reflecting the dissolution of secondary coarse oxide phases rather than grain coating oxy-hydroxides. Approximately 30% of the minerals dissolved are Fe-oxides, along with some clays and residual dolomite. A moderate correlation (R^2=0.34) between Fe and S suggests dissolution of minor pyrite; however a Fe/S ratio of $\approx$100 precludes pyrite dissolution as the dominant control on the Fe content of the leachate solution. The hydrochloric acid leach dissolves residual carbonate and oxide phases, and minor silicates. A larger fraction of total Fe is released in unaltered samples in this step, reflecting partial dissolution of the grain coating oxy-hydroxide phases.

3.1.1. Location of re-deposited metals

The results of the sequential extraction experiments are typified by cobalt (Co; Fig. 4). In both bleached and unbleached samples where no enrichment is observed, Co is released from carbonate, oxides and by dissolution of the residue (Fig. 4a), indicating that the trace metals are equally distributed between carbonate, coarse oxides and grain coating phases. In samples with bulk rock Co enrichment, the Co released in the steps dissolving carbonate and oxide phases is two orders of magnitude greater than background values (Fig. 4b). Re-deposited trace metals are therefore incorporated into the secondary oxide and carbonate phases growing at the bleaching reaction front [*Wigley et al.*, 2012].

3.2. Fraction of mobilized metals re-deposited

The minimum fraction of each trace metal re-deposited can be calculated from bleached halos surrounding fractures where the displacement distance of the reaction front is given by the perpendicular distance of the front from the fracture. The theoretical mass of a metal mobilized along a 1-dimensional path is given by the difference between the background concentrations in the red and bleached sandstones, and the displacement distance. The ratio of the predicted to observed mass of metal in the enriched zone gives a measure of the fraction of that metal re-deposited at the reaction front.

Some metals analyzed (Cu, V1; Zn, V2 and V3) exhibit re-deposited fractions close to unity, with the adsorbed mass being within error of the total mass dissolved (Table 2). Others (Cu, V2 and V3; Co, V1) show enrichment relative to the mass dissolved by propagation of the reaction front from the fracture. We consider that the true value lies in the upper range of calculated results as the sampling may have missed peaks in concentration, thus underestimating the mass of metal that has been re-deposited. Fluids entering the open fractures have previously reacted with unaltered rock and therefore may

be enriched in some metals and these, along with those mobilized by the reaction front moving away from the fracture, are all re-deposited.

Metals in solution exist either as free metal cations or metal-anion complexes (e.g. with OH^-, HCO_3^- or Cl^-). Speciation modeling using the calculated range in P_{CO2} and salinity and assuming that the fluid is buffered to equilibrium with calcite, suggests that Sn, Zn and Co exist as uncomplexed species, with a minor fraction of Co and Zn complexing with chloride and Zn also forming carbonate complexes (Supplementary figure 2); Cu speciation is dominated by chloride species. Realistic variations in methane concentrations do not significantly change calculated metal speciation profiles. Modelling was conducted using PHREEQC [Parkhurst and Appelo, 1999] with the llnl database [Johnson, 2000]. These calculations show that metal complexation does not play a major role in the re-deposition process, as metals complexing with hydroxyl, carbonate and chloride anions as well as free metal cations are all re-deposited at the CO_2-promoted reaction fronts.

Transport of mobilized metals is thus controlled by the distance moved by CO_2-promoted reaction fronts, rather than by the distance moved by the fluid. The difference between these length scales is controlled by the stoichiometry and kinetics of the fluid-rock reactions, and therefore the chemistry and mineralogy of the host formation. In non-reactive reservoirs mobilized metals will be transported further; however such reservoirs are less likely to contain significant quantities of contaminants.

3.3. Vertical transport distances across sub-horizontal reaction fronts

The observation that the metals removed from the bleached sandstone are quantitatively re-deposited can be used to calculate minimum transport distances perpendicular to the horizontal reaction fronts. The length of rock bleached by the fluid interacting

with horizontal reaction fronts has been calculated using the difference in background concentration in bleached and unbleached samples (mol.m^{-3}) and the mass of each metal deposited at the reaction front (mol.m^{-2}), assuming 100% re-deposition (l=M/ΔC; where l is the length of rock bleached, M is the mass of the metal in the enrichment (mol/m^2 reaction front) and ΔC is the difference in background concentrations between red and bleached sandstone). Some of the metals may have been removed by the sub-horizontal advection of the gravity current although this flux may decrease near the margin of a gravity current. If so the calculation underestimates the transport distance. Four transects across horizontal reaction fronts were analyzed (H1-4; localities in supplementary table 2), and the length of rock bleached for each unit area of reaction front is low (<0.35m; Fig. 5), consistent with the CO_2-rich fluid migrating laterally as a gravity current with vertical motion is dominated by diffusive processes except in the region of open fractures.

3.4. Potential impact on water quality

The TIFF (the volume of fluid that has interacted with the reaction front) has been calculated from the retardation factor (R) and the distance the front is displaced (Table 2). R is defined as the volume of fluid required to displace the reaction front through a unit volume of rock, and is estimated from the reaction stoichiometry and change in brine-CO_2 concentration across the reaction front [*Wigley et al.*, 2012]. TIFF is then given by R×distance, i.e. the volume of fluid required to displace the reaction front through the observed volume of rock.

Metal concentrations in the fluid (C_m) as the reaction front is displaced are given by:

$$C_m = \frac{F_m}{F_f} \quad (1)$$

where F_m is the flux of the metal (mol.m^{-2}.s^{-1}), and F_f is the fluid flux (m.s^{-1}). The time averaged metal flux is given by the mass of metal in the enrichment (mol/m^2 reaction front); and the corresponding F_f is given by the TIFF (Table 2).

Concentrations of Cu and Zn in solution are an order of magnitude below the World Health Organization (WHO) drinking water limit (Cu: 2 mg/L, Zn: 5mg/L; *WHO*, 2011) and Sn concentrations are well below acceptable limits (150 mg/L; *WHO*, 2003). No guidelines exist for Co; however calculated Co concentrations are 10 times the average composition of US freshwater [*ATSDR*, 1992] (see appendix A for a worked example).

4. Concluding remarks

The reaction fronts studied here, where fluid velocities are low and diffusive processes are important, have a high Damköhler number (N_D; the ratio of reaction rate to rate of advection) and a low Peclet number (Pe; the ratio of advective to diffusive transport). The high injection pressures in CO_2-storage reservoirs will result in high rates of advection and consequently such CO_2-promoted reaction fronts will have a lower N_D and a higher Pe compared to those documented here. However much of the concern over contaminant mobilization relates to migration of CO_2 from storage reservoirs into overlying aquifers where the groundwater flow rates are likely to be considerably lower (Fig. 6), being dominated by regional gradients in hydraulic head, such that CO_2-promoted reaction fronts have a transport characteristic comparable to those studied here. In this context, our results show that mobilized metals are likely to be re-deposited over small length scales in secondary carbonate and oxide phases precipitating at the CO_2-promoted reaction fronts. Fluxes of CO_2-charged waters of order of 25 times the volume of an aquifer of

the composition of the Entrada sandstone would be required for reaction fronts to pass through the aquifer, and for mobile trace metals to be extracted.

Acknowledgments. MW would like to thank Jason Day for advice with sequential leaching and geochemical analyses. Carbon research at Cambridge is supported by Natural Environment Research Council grant NE/F004699/1, part of the UK CRIUS (Carbon Research into Underground Storage) consortium. Niko Kampman is a recipient of financial support from Shell International. The manuscript was significantly improved as a result of comments by two anonymous reviewers.

Appendix A: Calculating metal concentrations in the fluid: a worked example

Calculation of the concentration of a metal in the fluid leaving the reaction front requires an estimate of the retardation factor of the formation and knowledge of the distance moved by the reaction front and the mass of the metal under consideration deposited at the reaction front.

The retardation factor, R, is given by:

$$\mathrm{R} = \frac{M_{\mathrm{hem}} . S}{\Delta \mathrm{CO}_2} \tag{A1}$$

where M_{hem} is the number of moles of hematite per m^3 formation ($\approx$40 moles), S is the number of moles of CO_2 needed to dissolve one mole of hematite ($\approx$3.2 moles; *Wigley et al.*, 2012) and ΔCO_2 is the change in CO_2 concentration in the fluid across the reaction front ($\approx$5 $\mathrm{mol/m}^3$; *Wigley et al.*, 2012). This gives a retardation factor of approximately 25.6.

The metal concentration is given by the metal flux divided by the fluid flux (Eqn. 1). By integrating over the duration of the bleaching event, this reduces to:

$$\text{Concentration} = \frac{M}{\text{TIFF}} \tag{A2}$$

where M is the mass of metal at the reaction front (Kg/m^2) and TIFF is the time integrated fluid flux (m^3/m^2), which is given by: R×X, where X is the distance moved by the reaction front.

The mass of copper deposited at reaction front V1 is 0.00152 Kg/m^2, and the reaction front has moved 0.506 m. The corresponding TIFF is therefore 13 m^3/m^2 and the concnetration of copper in the fluid as the reaction front propagates is 0.000312 kg/m^3 or 0.31 mg/L.

References

Assayag, N., M. Bickle, N. Kampman, and J. Becker (2009), Carbon Isotopic Constraints on CO_2 Degassing in Cold-Water Geysers, Green River, Utah, *Energy Procedia*, *1*(1), 2361 – 2366, doi:10.1016/j.egypro.2009.01.307, Greenhouse Gas Control Technologies 9: Proceedings of the 9th International Conference on Greenhouse Gas Control Technologies (GHGT-9), 20 November 2008, Washington DC, USA.

Beitler, B., M. A. Chan, and W. T. Parry (2003), Bleaching of Jurassic Navajo Sandstone on Colorado Plateau Laramide highs: Evidence of exhumed hydrocarbon supergiants?, *Geology*, *31*(12), 1041–1044, doi:10.1130/G19794.1.

Beitler, B., W. Parry, and M. A. Chan (2005), Fingerprints of Fluid Flow: Chemical Diagenetic History of the Jurassic Navajo Sandstone, Southern Utah, U.S.A., *Journal of Sedimentary Research*, *75*(4), 547–561, doi:10.2110/jsr.2005.045.

Benjamin, M. M., and J. O. Leckie (1981), Multiple-site Adsorption of Cd, Cu, Zn, and Pb on Amorphous Iron Oxyhydroxide, *Journal of Colloid and Interface Science*, *79*(1), 209 – 221, doi:10.1016/0021-9797(81)90063-1.

Bickle, M. J. (2009), Geological Carbon Storage, *Nature Geoscience*, *2*(12), 815–818, doi:10.1038/ngeo687 .

Bickle, M. J., and J. Baker (1990), Advective-Diffusive Transport of Isotopic Fronts: An Example from Naxos, Greece, *Earth and Planetary Science Letters*, *97*(12), 78 – 93, doi:10.1016/0012-821X(90)90100-C.

Bradl, H. B. (2004), Adsorption of Heavy Metal Ions on Soils and Soils Constituents, *Journal of Colloid and Interface Science*, *277*(1), 1 – 18, doi:10.1016/j.jcis.2004.04.005.

Rosso, K., and R. Bodnar (1995), Microthermometric and Raman Spectroscopic Detection limits of CO_2 in Fluid Inclusions and the Raman Spectroscopic Characterization of CO_2, *Geochimica et Cosmochimica Acta*, *59*(19), 3961 – 3975, doi:10.1016/0016-7037(95)94441-H.

Cullers, R. L. (1995), The Controls on the Major- and Trace Element Evolution of Shales, Siltstones and Sandstones of Ordovician toTertiary age in the Wet Mountains Region, Colorado, U.S.A., *Chemical Geology*, *123*(1-4), 107 – 131, doi:DOI: 10.1016/0009-2541(95)00050-V.

Dockrill, B., and Z. K. Shipton (2010), Structural Controls on Leakage from a Natural CO_2 Geologic Storage Site: Central Utah, U.S.A., *Journal of Structural Geology*, *32*(11), 1768 – 1782, doi:10.1016/j.jsg.2010.01.007.

Dubacq, B., M. Bickle, M. Wigley, N. Kampman, C. Ballentine, and B. Sherwood-Lollar (2012), Noble Gas and Carbon Isotopic Evidence for CO_2-driven Silicate Dissolution

in a Recent Natural CO_2 Field, *Earth and Planetary Science Letters*, *341-344*, 10-19, doi:10.1016/j.epsl.2012.05.040.

Agency for Toxic Substances and Disease Registry, (2004), Toxicological Profile for Cobalt. Atlanta, GA: U.S. Department of Health and Human Services, Public Health Service.

Förstner, U. (1982), Accumulative Phases for Heavy Metals in Limnic Sediments, *Hydrobiologia*, *91-92*, 269–284, doi: 10.1007/BF02391944.

Gale, J. (2004), Geological Storage of CO_2: What do we Know, Where are the Gaps and What More Needs to be Done?, *Energy*, *29*(9-10), 1329 – 1338, doi: 10.1016/j.energy.2004.03.068, 6th International Conference on Greenhouse Gas Control Technologies.

Johnson, J. Anderson G. Parkhurst D. Database 'thermo.com.v8.r6.230'. Rev. 1.11, Lawrence Livermore Natl. Lab., Livermore, California, 2000.

Kampman, N., M. Bickle, J. Becker, N. Assayag, and H. Chapman (2009), Feldspar Dissolution Kinetics and Gibbs Free Energy Dependence in a CO_2-enriched Groundwater System, Green River, Utah, *Earth and Planetary Science Letters*, *284*(34), 473 - 488, doi:10.1016/j.epsl.2009.05.013.

Kampman, N., N. M. Burnside, Z. K. Shipton, H. J. Chapman, J. A. Nicholl, R. M. Ellam, and M. J. Bickle (2012), Pulses of Carbon Dioxide Emissions from Intracrustal Faults Following Climatic Warming, *Nature Geoscience*, *5*, 352 – 358, doi:10.1038/ngeo1451 .

Keating, E., J. Fessenden, N. Kanjorski, D. Koning, and R. Pawar (2010), The Impact of CO_2 on Shallow Groundwater Chemistry: Observations at a Natural Analog Site and Implications for Carbon Sequestration, *Environmental Earth Sciences*, *60*, 521–536, 10.1007/s12665-009-0192-4.

Kharaka, Y., J. Thordsen, E. Kakouros, G. Ambats, W. Herkelrath, S. Beers, J. Birkholzer, J. Apps, N. Spycher, L. Zheng, R. Trautz, H. Rauch, and K. Gullickson (2010), Changes in the Chemistry of Shallow Groundwater Related to the 2008 Injection of CO_2 at the ZERT Field Site, Bozeman, Montana, *Environmental Earth Sciences*, *60*, 273–284, 10.1007/s12665-009-0401-1.

Little, M. G., and R. B. Jackson (2010), Potential Impacts of Leakage from Deep CO_2 Geosequestration on Overlying Freshwater Aquifers, *Environmental Science and Technology*, *44*(23), 9225–9232, doi:10.1021/es102235w.

Lu, J., J. Partin, S. Hovorka, and C. Wong (2010), Potential Risks to Freshwater Resources as a Result of Leakage from CO_2 Geological Storage: a Batch-Reaction Experiment, *Environmental Earth Sciences*, *60*, 335–348, 10.1007/s12665-009-0382-0.

Intergovernmental Panel on Climate Change, (2007), *Fourth Assessment Report: Climate Change 2007: Working Group I Report: The Physical Science Basis*, Geneva: IPCC.

D. L. Parkhurst and C. A. J. Appelo. User's Guide to PHREEQC (version 2) - A Computer Program for Speciation, Batch-Reaction, One-Dimensional Transport, and Inverse Geochemical Calculations. (Water-Resources Investigations Report 99-4259), 1999.

World health Organization (2003), Hydrogen Sulfide in Drinking Water. Background Document for Preparation of WHO Guidelines for Drinking Water Quality. Report no. WHO/SDE/WSH/03.04/07

World health Organization (2011), Guidelines for Drinking-Water Quality. ISBN: 92 4 154696 4.

Smyth, R. C., S. D. Hovorka, J. Lu, K. D. Romanak, J. W. Partin, C. Wong, and C. Yang (2009), AssessingRisk to Fresh Water Resources from Long Term CO_2

Injection-Laboratory and Field Studies, *Energy Procedia*, *1*(1), 1957 – 1964, doi: 10.1016/j.egypro.2009.01.255, Greenhouse Gas Control Technologies 9, Proceedings of the 9th International Conference on Greenhouse Gas Control Technologies (GHGT-9), 16-20 November 2008, Washington DC, USA.

Tessier, A., P. G. C. Campbell, and M. Bisson (1979), Sequential Extraction Procedure for the Speciation of Particulate Trace Metals, *Analytical Chemistry*, *51*(7), 844–851, doi:10.1021/ac50043a017.

Trimble, L. (1978), *Geology and Uranium-Vanadium Deposits of the San Rafael River Mining Area, Emery County, Utah.*, vol. 113, Utah Geological and Mineral Survey.

Wigley, M., N. Kampman, B. Dubacq, and M. Bickle (2012), Fluid-Mineral Reactions and Trace Metal Mobilization in an Exhumed Natural CO_2 Reservoir, Green River, Utah, *Geology*, *40*, 555-558, doi:10.1130/G32946.1.

Wigley, M., B. Dubacq, N. Kampman, and M. Bickle (In Press), Controls on Sluggish, CO_2-promoted Hematite and K-feldspar Dissolution Kinetics in Sandstones, *Earth and Planetary Science Letters*, -, -, doi:-.

Wilkin, R. T., and D. C. DiGiulio (2010), Geochemical Impacts to Groundwater from Geologic Carbon Sequestration: Controls on pH and Inorganic Carbon Concentrations from Reaction Path and Kinetic Modeling, *Environmental Science and Technology*, *44*(12), 4821–4827, doi:10.1021/es100559j, pMID: 20469895.

Yin, Y., H. E. Allen, Y. Li, C. P. Huang, and P. F. Sanders (1996), Adsorption of Mercury(II) by Soil: Effects of pH, Chloride, and Organic Matter, *Journal of Environmental Quality*, *25*(4), 837–844, doi:10.2134/jeq1996.00472425002500040027x.

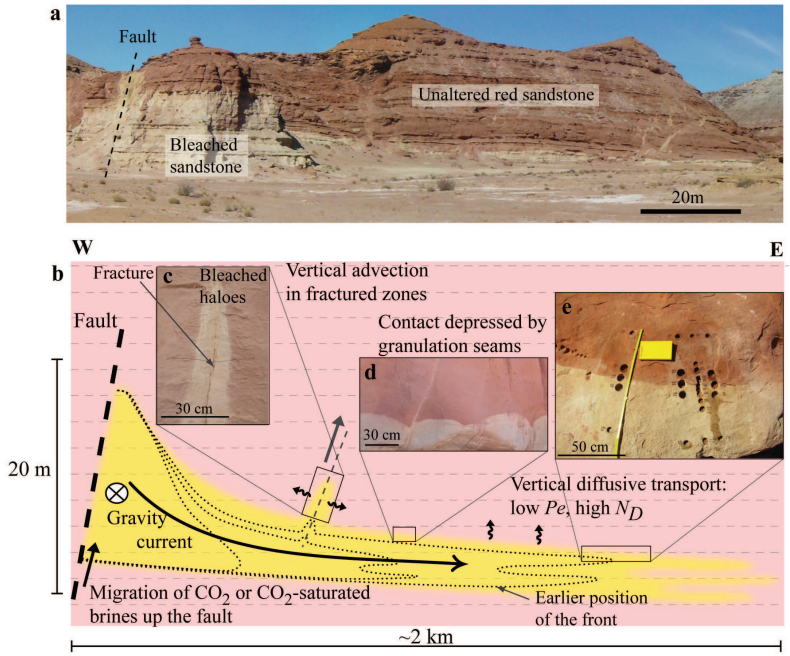

Figure 1. Illustration and outcrop photos of the exhumed CO_2 reservoir. (a) Bleaching at the crest of the anticline, facing north. (b) Schematic development of bleached sandstone (yellow) in original sandstones (red). CO_2 (or CO_2-rich brine) migrated into the formation near the crest of the Green River anticline along faults and flowed laterally as a gravity current. A CO_2-promoted bleaching front (dotted lines) propagated laterally by advection and vertically by diffusion. The preserved reaction front is sub-horizontal and exhibits cuspate regions associated with open fractures and granulation seams (d). Bleached halos develop around vertical fractures (c). (e) Sampling across sub-horizontal reaction fronts. Modified from Wigley et al; In Press

Zheng, L., J. A. Apps, Y. Zhang, T. Xu, and J. T. Birkholzer (2009), On Mobilization of Lead and Arsenic in Groundwater in Response to CO_2 Leakage from Deep Geological Storage, *Chemical Geology*, *268*(3-4), 281 – 297, doi:10.1016/j.chemgeo.2009.09.007.

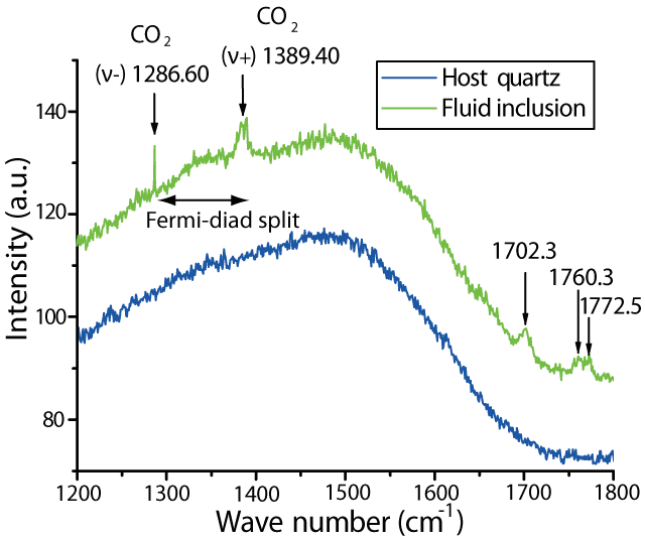

Figure 2. Close up of the region 1200-1800 cm^{-1} for the Raman spectra of the host and the vapour phase of a fluid inclusion in a quartz overgrowth from bleached Entrada sandstone. The CO_2 peaks are marked, along with the Fremi-diad split which is used to calculate a range in CO_2 partial pressures in the bleaching fluid.

Table 1. Mol fractions of minerals released in each sequential leaching step[a]

	Average mol fraction released				
	MΩ water rinse	Exchangeable leach	Carbonate leach	Oxide leach	HCl leach
Quartz	0.00 (0)	0.02 (1)	0.00 (0)	0.03 (1)	0.00 (0)
K-feldspar	0.10 (2)	0.17 (6)	0.01 (1)	0.12 (5)	0.01 (1)
Plagioclase	0.00 (0)	0.00 (0)	0.00 (0)	0.00 (0)	0.01 (0)
Clay	0.07 (1)	0.19 (7)	0.01 (0)	0.34 (12)	0.04 (1)
Calcite	0.04 (1)	0.23 (8)	0.63 (5)	0.00 (0)	0.84 (24)
Dolomite	0.05 (1)	0.05 (2)	0.18 (1)	0.17 (6)	0.04 (1)
Fe-dolomite	0.00 (0)	0.01 (0)	0.14 (1)	0.00 (0)	0.00 (0)
Hematite	0.00 (0)	0.00 (0)	0.01 (0)	0.29 (11)	0.06 (2)
Pyrite	0.00 (0)	0.00 (0)	0.00 (0)	0.04 (2)	0.00 (0)
Gypsum	0.73 (12)	0.34 (13)	0.02 (0)	0.00 (0)	0.00 (0)
TiO_2	0.00 (0)	0.00 (0)	0.00 (0)	0.00 (0)	0.00 (0)

[a] Numbers in parentheses are 1 σ uncertainties for the last digit, calculated from the magnitude of the misfit to bulk rock values.

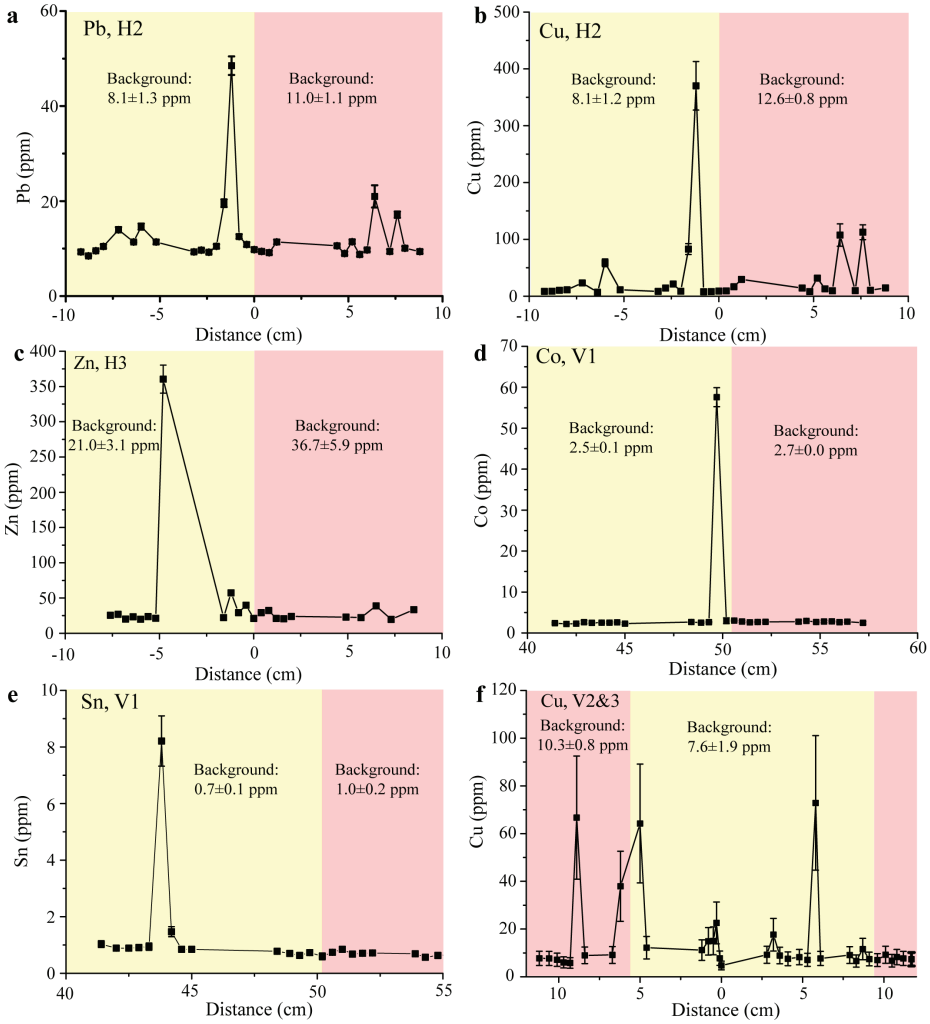

Figure 3. Concentration profiles for selected metals across horizontal reaction fronts (a-c, distances from the red-bleached transition) and fracture associated reaction fronts (d-f, distances from the core of the fracture). Red color denotes unaltered rock, yellow is bleached sandstone. a) Pb, H2; b) Cu, H2; c) Zn, H3; d) Co, V1; e) Sn, V1; f) Cu either side of a bleached fracture (V2 and V3, V2 negative). Background concentrations in red and bleached rock are indicated. Error bars show 2σ propagated uncertainties including recovery relative to USGS standard Sco-1, repeat averages and instrument uncertainties.

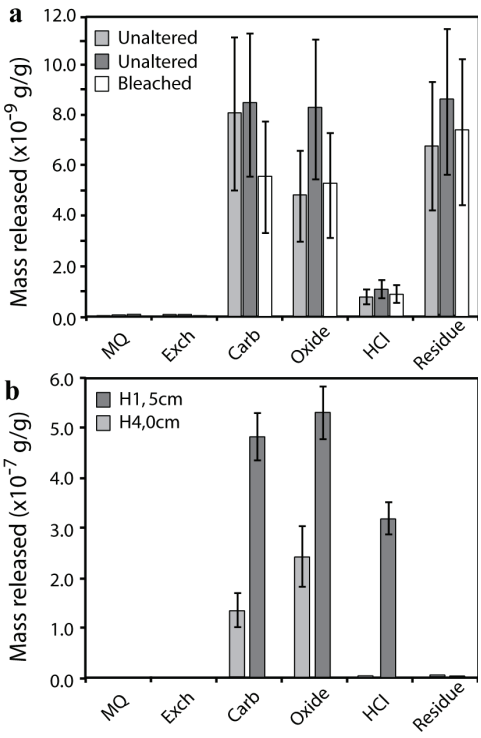

Figure 4. Results of sequential leaching for Co. a) Mass of Co released in 3 samples without: 2 samples of unaltered sandstone and 1 sample of bleached sandstone 50cm below the reaction front. Co is widely distributed between phases. b) Mass of Co released in each leaching step for two samples which show enrichment in Co. Transect name, and distance from the red-bleached transition are given (positive numbers indicate unaltered rock). Note the different scales on the two graphs. Error bars are 2σ propagated recoveries relative to bulk rock concentrations and instrument uncertainties. Major and trace element composition of leaches are given in supplementary table 3.

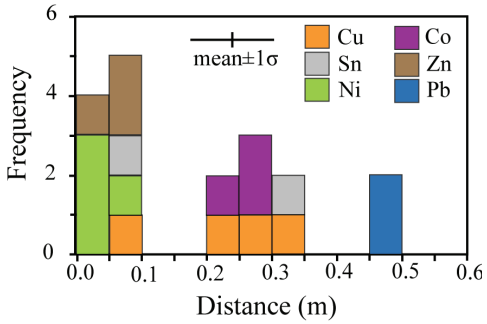

Figure 5. Calculated vertical distances moved by the sub-horizontal bleaching reaction front. Colors represent calculations of different metal enrichments. Uncertainties are 1σ of background uncertainties in red and bleached sandstone propagated with peak height uncertainties.

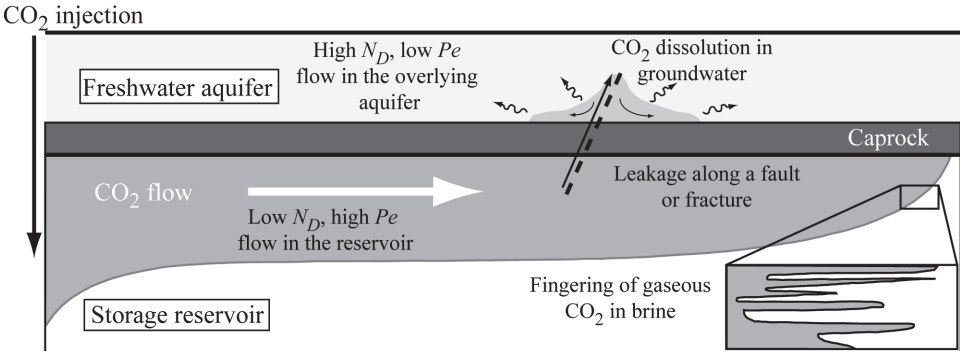

Figure 6. Schematic description of a CO_2 injection site. If CO_2 migrates into overlying groundwater systems with low natural fluid flow rates, conditions may be similar to those in the Green River analogue site where the low transport rates mean that reaction fronts retard the potential transport of metals. Modified from [*Dubacq et al.*, 2012].

Table 2. Enrichment factors, fractions of each metal re-deposited, TIFF and maximum possible fluid concentrations at the fracture associated bleaching reaction fronts [b]

Metal	Transect	Advective distance (m)	Enrichment factor	Fraction re-deposited	TIFF (m^2/m^3)	Enriched zone width (m)	Av. fluid concentration (mg/L)
Cu	V1	0.19	18 (1)	0.6 (4)	4.9	0.006	0.312
	V2	0.10	20 (5)	2.8 (20)	3.5	0.01	0.283
	V3	0.14	7 (2)	3.4 (24)	2.4	0.006	0.283
Zn	V2	0.06	8 (3)	0.9 (5)	1.4	0.008	0.417
	V3	0.07	3 (1)	1.3 (8)	1.8	0.008	0.417
Co	V1	0.88	21 (1)	2.8 (17)	22.5	0.006	0.016
Sn	V1	0.11	12 (3)	0.4 (3)	2.7	0.006	0.034

[b] Numbers in parentheses are 1σ uncertainties on the last digit. Uncertainties for fraction re-adsorbed and enrichments are 1σ of background uncertainties in red and bleached sandstone propagated with peak height uncertainties.